01 Mar 2002

Analytical Derivation of a Coupled-circuit Model of a Claw-pole Alternator with Concentrated Stator Windings

Hua Bai

Steven Pekarek
Missouri University of Science and Technology

Jerry L. Tichenor

Walter Eversman
Missouri University of Science and Technology, eversman@mst.edu

et. al. For a complete list of authors, see https://scholarsmine.mst.edu/mec_aereng_facwork/3322

Recommended Citation

H. Bai et al., "Analytical Derivation of a Coupled-circuit Model of a Claw-pole Alternator with Concentrated Stator Windings," *IEEE Transactions on Energy Conversion*, Institute of Electrical and Electronics Engineers (IEEE), Mar 2002.
The definitive version is available at https://doi.org/10.1109/60.986434

Analytical Derivation of a Coupled-Circuit Model of a Claw-Pole Alternator With Concentrated Stator Windings

Hua Bai, *Student Member, IEEE*, Steven D. Pekarek, *Member, IEEE*, Jerry Tichenor, *Member, IEEE*, Walter Eversman, Duane J. Buening, Gregory R. Holbrook, Michael L. Hull, Ronald J. Krefta, and Steven J. Shields

***Abstract*—A lumped-parameter coupled-circuit model of a claw-pole alternator is derived. To derive the model, analytical techniques are used to define a three-dimensional (3-D) Fourier-series representation of the airgap flux density. Included in the series expansion are the harmonics introduced by rotor saliency, concentrated stator windings, and stator slots. From the airgap flux density waveform, relatively simple closed-form expressions for the stator and rotor self- and mutual-inductances are obtained. The coupled-circuit model is implemented in the simulation of an alternator/rectifier system using a commercial state-model-based circuit analysis program. Comparisons with experimental results demonstrate the accuracy of the model in predicting both the steady-state and transient behavior of the machine.**

***Index Terms*—Fourier series, power conversion harmonics, synchronous machines, torque measurement.**

I. Introduction

CLAW-POLE, or so-called "Lundell" alternators are often used as the power source in finite inertia systems, including automobiles and aircraft. Although of similar function, the Lundell alternator is different than machines used in bulk-power utility applications. In particular, the rotor poles are shaped in the form of claws and the field winding is wound concentrically around a cylindrical rotor core. In addition, to minimize cost, many Lundell machines are constructed using concentrated stator windings (1 slot/pole/phase).

Over the past several decades significant effort has been placed on deriving circuit-based models of standard synchronous machines that can be used to evaluate machine and system performance. Although reasonably accurate for standard machines, due to the claw-type rotor geometry and the use of concentrated stator windings, these equivalent-circuit representations are limited in their ability to characterize the dynamics of Lundell machines. In particular, a Park's circuit cannot be readily used to determine voltage or current harmonics that result from the claw design or a nonsinusoidal winding distribution. To obtain an accurate model most analysts have relied on finite element (FE) analysis [1]–[4]. Although FE techniques have been shown to be effective, the computation time required to obtain a state model can limit their utility. For example, once a mesh has been generated it requires over 8 h of CPU time on a 2×552 MHz processor workstation to derive the model of a claw-pole machine using a three-dimensional (3-D) FE approach [5]. Thus, although valuable in final-stage design verification, an FE approach is inefficient for design iterations that may include selecting winding patterns, pitch and skew angles, or claw geometry.

As an alternative, some analysts have chosen magnetic equivalent circuit (MEC) analysis to establish models of the Lundell alternator [6], [7]. In a MEC approach, the principal flux paths are identified and a magnetic circuit is established that relates winding currents to flux in all parts of the machine. Although a valuable tool, significant experience is required to formulate the model and structure it in a form compatible with commercial circuit-analysis software. Further, due to the complex geometry of the rotor claw, partitioning the claw segments and establishing closed-form permeance expressions for the segmented sections requires considerable effort. In addition, to model the magnetic circuit requires the solution of a sizeable system of algebraic equations at each numerical time step.

In this paper, analytical techniques are used to derive a fourth-order coupled-circuit model of a three-phase Lundell alternator. To derive the model, a 3-D Fourier-series representation of the airgap flux density is established. Included in the series expansion are the harmonics that are introduced by rotor saliency, concentrated stator windings, and stator slots. The airgap flux density waveform is used to obtain closed-form expressions of the self- and mutual-inductances that are easily incorporated in commercial circuit-analysis software. Although several assumptions are required to develop the model, it is reasonably accurate and provides an efficient means to evaluate the performance of a claw-pole machine in complex power systems. In addition, machine dimensions, winding configuration, skew and pitch angles, and claw geometry are easily modified to investigate alternative machine designs. To demonstrate its utility, the coupled-circuit model is implemented in the simulation of a six-pulse alternator/rectifier system using a state-model-based circuit analysis program. Comparisons with experimental results demonstrate the accuracy of the model in predicting the steady state and transient performance of the system.

Manuscript received April 2, 2001.

H. Bai, S. D. Pekarek, J. Tichenor, and W. Eversman are with the Department of Electrical and Computer Engineering, University of Missouri-Rolla, Rolla, MO 65409-1060 USA. W. Eversman is also with the Department of Mechanical and Aerospace Engineering and Engineering Mechanics, University of Missouri-Rolla, Rolla, MO 65409-1060 USA (e-mail: pekarek@ece.umr.edu).

D. J. Buening, G. R. Holbrook, M. L. Hull, R. J. Krefta and S. J. Shields are with Delphi Automotive Systems, Troy, MI 48098 USA.

Publisher Item Identifier S 0885-8969(02)01513-9.

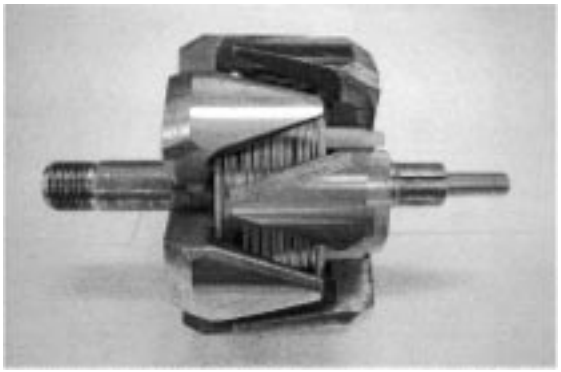

Fig. 1. Rotor structure of claw-pole alternator.

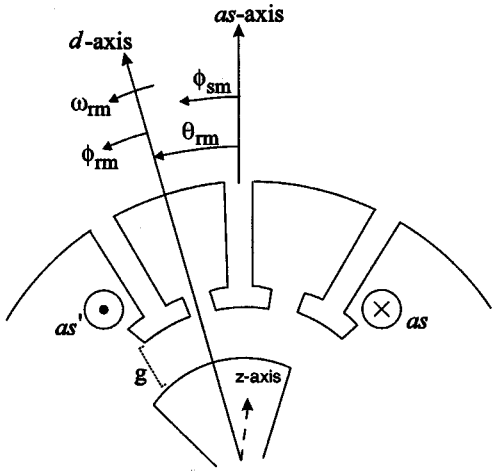

Fig. 2. Illustration of reference axes, angles, and dimensions.

II. Definitions, Assumptions, and Model Description

The machine modeled has three wave-wound concentrated stator windings, 12 poles, 36 stator slots, and rotor poles shaped in the form of a claw. The rotor structure is shown in Fig. 1. A simplified diagram of a single pole of the stator/rotor with the angles and dimensions that are used in the machine analysis is shown in Fig. 2. They are defined as follows.

ϕ_{sm}	Angular position on the stator relative to as-axis.
ϕ_{rm}	Angular position on the rotor relative to d-axis.
θ_{rm}	Angular position between as- and d-axis.
ω_{rm}	Rotor angular velocity (rad/s).
g	Length of airgap.
z	Axial position in the airgap.
l	Axial length of stator.
N_s	Number of conductors in a stator slot.
N_{fd}	Number of turns of the field winding.
r	Radius from center of rotor core to the midpoint of the airgap.

In general, models of electrical machinery are expressed in terms of so-called "electrical" angles and angular velocities. These are defined as

$$\phi_s = \frac{P}{2}\phi_{sm} \tag{1}$$

$$\phi_r = \frac{P}{2}\phi_{rm} \tag{2}$$

$$\theta_r = \frac{P}{2}\theta_{rm} \tag{3}$$

$$\omega_r = \frac{P}{2}\omega_{rm} \tag{4}$$

where P is the number of poles.

The coupled-circuit model is structured with the electrical dynamics of the stator and rotor circuits represented in a form

$$\begin{bmatrix} \mathbf{v}_{abcs} \\ v_{fd} \end{bmatrix} = \begin{bmatrix} \mathbf{r}_s & 0 \\ 0 & r_{fd} \end{bmatrix} \begin{bmatrix} \mathbf{i}_{abcs} \\ i_{fd} \end{bmatrix} + p \begin{bmatrix} \lambda_{abcs} \\ \lambda_{fd} \end{bmatrix} \tag{5}$$

$$\begin{bmatrix} \lambda_{abcs} \\ \lambda_{fd} \end{bmatrix} = \begin{bmatrix} \mathbf{L}_{ss}(\theta_r) & \mathbf{L}_{sfd}(\theta_r) \\ \mathbf{L}_{fds}(\theta_r) & L_{fdfd}(\theta_r) \end{bmatrix} \begin{bmatrix} \mathbf{i}_{abcs} \\ i_{fd} \end{bmatrix} \tag{6}$$

where v, i, and λ represent voltage, current, and flux linkages of respective windings and $p = d/(dt)$. The matrices $\mathbf{L}_{ss}(\theta_r)$, $\mathbf{L}_{sfd}(\theta_r)$, and $\mathbf{L}_{fds}(\theta_r)$ contain the self- and mutual-inductances between respective windings. The scalar $L_{fdfd}(\theta_r)$ represents the self-inductance of the field winding.

The dynamics of the rotor are represented in state model form as

$$p\omega_r = \frac{P}{2J}(T_e - T_{\text{in}}) \tag{7}$$

$$p\theta_r = \omega_r \tag{8}$$

where T_{in} is the input torque applied to the rotor, J the rotor inertia, and T_e the electromagnetic torque. The electromagnetic torque can be expressed in terms of the co-energy of the coupling field as [8]

$$T_e = \frac{P}{2}\frac{\partial W_c}{\partial \theta_r} \tag{9}$$

where

$$W_c = \frac{1}{2}\left[\mathbf{i}_{abcs} i_{fd}\right] \begin{bmatrix} \mathbf{L}_{ss}(\theta_r) & \mathbf{L}_{sfd}(\theta_r) \\ \mathbf{L}_{fds}(\theta_r) & L_{fdfd}(\theta_r) \end{bmatrix} \begin{bmatrix} \mathbf{i}_{abcs} \\ i_{fd} \end{bmatrix}. \tag{10}$$

In order to derive the coupled-circuit model, it is assumed that 1) the iron is of sufficiently high permeability that the drop in magnetic potential across stator and rotor can be neglected and 2) only the radial component of the flux density is modeled in the airgap, yielding

$$\vec{\mathbf{B}}_{\text{air}} = B_{\text{air}}(\phi_s, \theta_r, z)\vec{\mathbf{a}}_r. \tag{11}$$

For simplicity, and without loss in generality, only the self- and mutual-inductances of the phase-*a* winding are derived herein. Thus, in subsequent sections B_{air} represents the airgap flux density resulting from energization of the phase-*a* winding.

III. Derivation of Coupled-Circuit Model

The critical components of the coupled-circuit model are the self- and mutual-inductances of the respective windings. Assuming a concentrated winding, the phase-*a* self-inductance can be expressed as the sum of a leakage inductance and an inductance that is obtained by integrating B_{air} over the surface spanned by a single coil of a single pole of the winding and multiplying by the number of coil turns and the number of pole

pairs. In particular, assuming a full-pitch winding with the angle ϕ_{sm} defined in Fig. 2 and $\phi_s = (P/2)\phi_{sm}$

$$L_{asas} = L_{ls} + N_s \frac{P}{2} \int_0^l \int_{-(\pi/2)}^{\pi/2} B_{\text{air}}(\phi_s, \theta_r, z)(r d\phi_s) dz \tag{12}$$

where B_{air} is normalized to the value of winding current and L_{ls} is defined as the stator leakage inductance. It is important to note that L_{ls} does not include what some analysts refer to as leakage due to winding harmonics. These are included within the integral in (12). Evaluation of L_{ls} is described in Section IV.

Neglecting end-turn mutual inductance, the phase-*b* to phase-*a* mutual inductance is found by integrating B_{air} over the surface spanned by a single coil of a single pole of the phase-*b* winding and multiplying the result by the number of coil turns and the pole pairs. In particular, for a full-pitch winding that is displaced from the phase-*a* winding by 120 electrical degrees

$$L_{bsas} = N_s \frac{P}{2} \int_0^l \int_{\pi/6}^{7\pi/6} B_{\text{air}}(\phi_s, \theta_r, z)(r d\phi_s) dz. \tag{13}$$

The field- to phase-*a* mutual-inductance is obtained by integrating the airgap flux density over the span of a single claw and multiplying by the number of field turns and pole pairs. Assuming the base of a claw spans 180 electrical degrees

$$L_{fdas} = N_{fd} \frac{P}{2} \int_0^l \int_{-(\pi/2)}^{\pi/2} B_{\text{air}}(\phi_r, \theta_r, z)(r d\phi_r) dz. \tag{14}$$

In machines with stator and rotor teeth that have uniform dimensions along the z-axis of the machine, the airgap flux density is often expressed in a form

$$B_{\text{air}} = MMF \cdot \gamma \tag{15}$$

where MMF is a magnetomotive force and γ is the airgap permeance, defined as the permeability of free space over the length of the airgap (μ_0/g) [8]. Changes in permeance that result from variance of the airgap length due to rotor saliency and stator slots are accounted for by expressing γ in terms of angular positions on the stator and rotor [14].

For a claw-pole machine it is difficult to represent the airgap flux density as an MMF multiplied by a single permeance function γ. In particular, not only is the airgap length a function of the circumferential position on the stator and rotor, the respective alignment of a stator tooth and a rotor claw is a function of the axial position z. To include the 3-D effects of rotor saliency and stator slots the airgap flux density is expanded in a form

$$B_{\text{air}}(\phi_r, \phi_s, z) = MMF_{as}(\phi_s)\gamma_r(\phi_r, z)sl(\phi_s) \tag{16}$$

where γ_r is an airgap permeance function that is used to account for changes in airgap length due to rotor saliency, and sl is a function that represents the reduction of the flux density around stator slots. It is noted that if slot harmonics are not of interest the reduction of the flux density due to stator slots can be approximated using a Carter-coefficient, in which case sl becomes a constant. However, in this analysis, the influence of the slot harmonics on the machine and system performance is approximated in more detail.

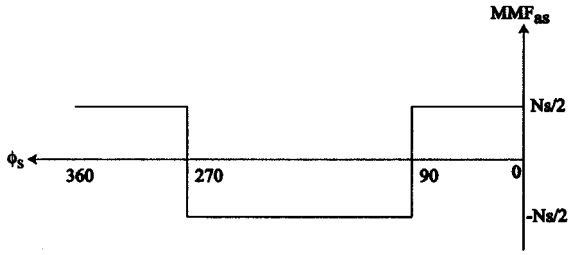

Fig. 3. MMF (normalized) of the phase-*a* winding.

Derivation of an expression for B_{air} is accomplished by evaluating the three terms on the right-hand side of (16) independently. Assuming concentrated stator windings, the magnetomotive force MMF_{as} can be represented as a square wave function as one traverses the stator of the machine. This is shown in Fig. 3, where a normalized MMF_{as} is plotted with respect to the electrical position on the stator ϕ_s. MMF_{as} is normalized to the value of stator current. In reality, the conductors are distributed across a slot opening, and, therefore, MMF_{as} may have a more gradual change than that represented by a square wave. However, this discrepancy has only a minor influence on determining the overall machine performance.

Since MMF_{as} is an even function with respect to ϕ_s, it can be represented in the form of a series as

$$MMF_{as}(\phi_s) = \frac{N_s}{2} \sum_{n=1}^{\infty} \sin\left(\frac{n\pi}{2}\right) \frac{4}{\pi n} \cos(n\phi_s). \tag{17}$$

To evaluate γ_r it is assumed that the airgap length between claws is sufficiently large that the airgap permeance is zero. Using this assumption, the permeance has two possible values

$$\gamma_r(\phi_r, z) = \begin{bmatrix} \frac{\mu_0}{g} \\ 0 \end{bmatrix} \begin{matrix} \text{above a rotor claw} \\ \text{between rotor claws.} \end{matrix} \tag{18}$$

The reliance on both the angular position ϕ_r and axial position z results from the claw structure. To establish a closed-form expression that represents (18) a one-dimensional (1-D) series evaluation is first considered. In particular, at any given axial position z it is possible to establish a Fourier-series representation of γ_r as a function of ϕ_r. To illustrate, the permeance versus the angular position on the rotor ϕ_r at the midpoint of the claw length $(z = l/2)$ is shown in Fig. 4. The angles a_1 and a_2 defined in Fig. 4 form the intervals of integration in the evaluation of the Fourier coefficients. Using these angles a series expression for the permeance at $(z = l/2)$ can be written

$$\gamma_r\left(\phi_r, \frac{l}{2}\right) = \sum_{k=0}^{\infty} \gamma_{ak}\left(\frac{l}{2}\right) \cos(k\phi_r) \tag{19}$$

where

$$\gamma_{ak}\left(\frac{l}{2}\right) = \frac{2}{\pi}\frac{\mu_0}{g}\left\{\int_0^{a_1} \cos(k\phi_r)d\phi_r + \int_{a_2}^{\pi} \cos(k\phi_r)d\phi_r\right\}. \tag{20}$$

In general, a 1-D series expansion for permeance can be defined at any axial position by rederiving expressions for the angles a_1 and a_2. Therefore, a 2-D Fourier-series expression for the permeance can be derived by establishing a closed-form expression relating a_1 and a_2 to z.

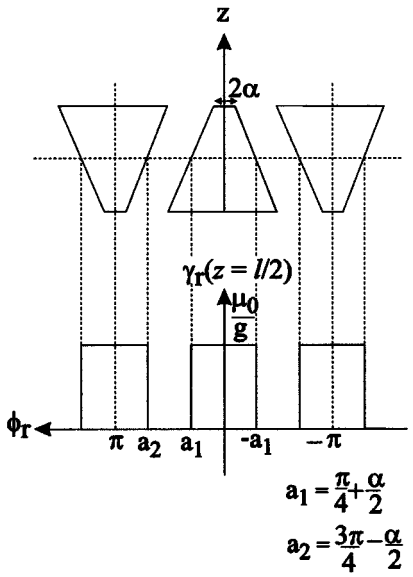

Fig. 4. Airgap permeance as a function of ϕ_r at $z = l/2$.

If the rotor is symmetric, and ϕ_r is defined from the d-axis, the angles are given by

$$a_1(z) = \frac{\pi}{2} - \frac{z\pi}{2l} + \frac{z\alpha}{l} \tag{21}$$

$$a_2(z) = \pi - \alpha - \frac{z\pi}{2l} + \frac{z\alpha}{l}. \tag{22}$$

Using (21) and (22) to evaluate the Fourier coefficients, a 2-D permeance can be expressed in a general form

$$\gamma_r(\phi_r, z) = \sum_{k=0}^{\infty} \gamma_{ak}(z)\cos(k\phi_r) + \sum_{k=1}^{\infty} \gamma_{bk}(z)\sin(k\phi_r) \tag{23}$$

where

$$\gamma_{a0} = \frac{\mu_0}{g\pi}(\pi + 2\alpha) \tag{24}$$

$$\gamma_{ak}(z) = \frac{2\mu_0}{k\pi g}\left(\sin\left(\frac{k}{2}\left(\pi - \frac{z\pi}{l} + \frac{2z\alpha}{l}\right)\right) + \sin\left(\frac{k}{2}\left(-2\pi + \frac{z\pi}{l} + 2\alpha - \frac{2z\alpha}{l}\right)\right)\right)$$

$$k \geq 1 \tag{25}$$

$$\gamma_{bk}(z) = 0. \tag{26}$$

The angle α is one-half the width at the tip of the claw as shown in Fig. 4. It is noted that close inspection of the claw structure in Fig. 1 shows chamfering of a single side of the claw producing a general asymmetry in the rotor structure. Although complicating the derivation slightly, asymmetries of the rotor are readily accounted for and result in only a slight change in the coefficients in (23).

The result of the multiplication of (17) and (23) is a representation of the airgap flux density around the machine at all angles except the location of stator slots. At the location of stator slots, the flux density is reduced. Methods of accounting for flux pulsation around stator teeth have been established using several analytical, graphical, and experimental techniques [13]. In the design of electric machines, the most common method is to multiply the actual airgap by a Carter coefficient to establish an effective airgap length. Although accurate, accounting for stator slots using an effective airgap length does not provide information regarding slot harmonics or cogging torque.

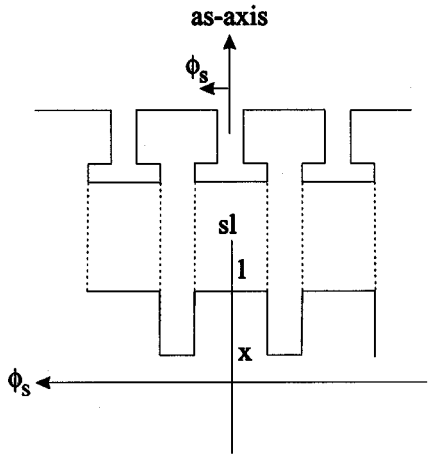

Fig. 5. Stator slot function.

To account for slot harmonics, a quasibinary slot function sl is used. The function is illustrated using the diagram shown in Fig. 5. sl is defined as having a value of 1 at the position where there is a tooth, and a value of x at the position at the location of a slot. The value of x represents the ratio of the flux density at the center of the slot to the flux density at the center of the stator tooth assuming a uniform rotor structure. Its value can be obtained from the graphical analysis of flux pulsation around slots [13]. For the machine modeled $x = 0.4$. It is noted that using this technique the average value of the slot function is equal to the Carter coefficient. In reality, the tips of the stator teeth may saturate, and the airgap flux density does not contain the abrupt transitions of a square wave. However, this approximation represents a worst case scenario in terms of slot harmonics and cogging torque amplitude. The slot function can be expanded in terms of a Fourier series as

$$sl(\phi_s) = \sum_{m=0}^{\infty} sl_{am}\cos(m\phi_s). \tag{27}$$

Multiplication of (17), (23), and (27) results in the expression for airgap flux density that is used in the evaluation of (12)–(14). Direct evaluation of the integrals is difficult due to the complexity of the series components. As an alternative, the solution can be found using numerical integration.

The numerical values can be used to establish lookup tables of inductance and derivatives of inductance versus rotor position. Alternatively, a curve-fitting routine can provide closed-form expressions of the self- and mutual-inductance. For the machine considered, curve-fits to the general forms

$$L_{asas} = L_{ls} + L_a + L_{b1}\cos(2\theta_r + \phi_{b1}) + L_{b2}\cos(4\theta_r + \phi_{b2}) \tag{28}$$

$$L_{bsas} = L_{am} + L_{bm1}\cos(2\theta_r + \phi_{bm1}) + L_{bm2}\cos(4\theta_r + \phi_{bm2}) \tag{29}$$

$$L_{fdas} = \sum_{k=1,3,5,7} L_{afk}\cos(k\theta_r + \alpha_k) \tag{30}$$

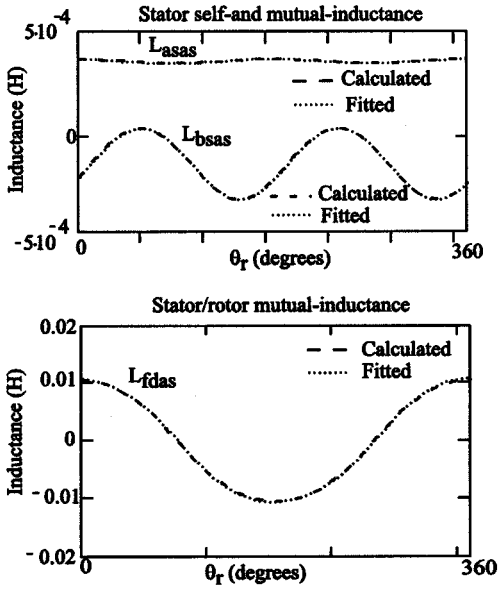

Fig. 6. Calculated and fitted stator self- and mutual-inductance.

were sufficient to approximate the numerically calculated stator self- and mutual-inductance and their respective derivatives. The fitted inductances are shown along with the calculated values in Fig. 6.

It is interesting to note that in the claw-pole machine with concentrated stator windings, the phase-*a* self-inductance is nearly constant with respect to rotor position. In contrast, the mutual-inductance has a much more significant variation. Typically, in the derivation of models of standard salient-pole machines, the amplitude of the variation of the self- and mutual-inductances with respect to rotor position is assumed to be equal, i.e., $L_{b1} = L_{bm1}$ [8]. Here the difference results from flux density harmonics introduced by the claw-pole saliency. It is also interesting to note that in standard machines $L_{am} \approx -L_a/2$ [8]. However, the harmonics introduced by the concentrated stator windings produce a relation $L_{am} \approx -L_a/3$. This difference becomes important when considering the stator leakage inductance.

IV. Leakage Inductance Calculations

The stator and field leakage inductances play an important role in the dynamic performance of the machine. To calculate the stator leakage inductance, standard expressions for slot and end turn leakage were applied [14]. The calculated value was found to be $L_{ls} = 0.175$ mH. Out of curiosity the stator leakage inductance was measured with the rotor in place using a two step experiment. As a first step, the zero-sequence inductance was determined.[1] By definition, the zero-sequence flux linkage is obtained by taking one-third the sum of the phase flux linkages

$$\lambda_{0s} = \frac{\lambda_{as} + \lambda_{bs} + \lambda_{cs}}{3}. \tag{31}$$

[1]Ideas for a zero-sequence test were obtained from discussions with Dr. S. D. Sudhoff of Purdue University.

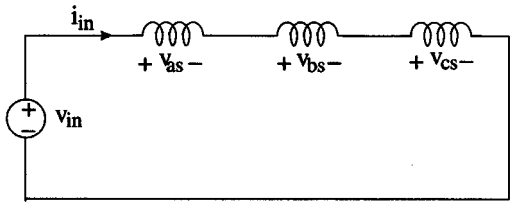

Fig. 7. Circuit for zero sequence inductance measurement.

From the derivations in Section III, adding the phase flux linkages results in the expression

$$\lambda_{0s} = \left(L_{ls} + \frac{L_a}{3}\right) i_{0s}. \tag{32}$$

To determine the value of zero-sequence inductance, step changes in input voltage were applied to series-tied stator windings as shown in Fig. 7. The input current was measured during the entire transient, providing an expression for the derivative of the zero-sequence flux linkage. In particular

$$p\lambda_{0s} = \frac{v_{\text{in}}}{3} - r_s i_{\text{in}}. \tag{33}$$

The steady-state zero-sequence flux linkage was obtained by the numerical integration of (33). The ratio of the calculated λ_{0s} versus measured i_{0s} provided the zero-sequence inductance. Using the calculated value of L_a, the measured leakage inductance was found to be 0.2 mH, which agreed reasonably well with the calculated value.

Using analytical expressions for the claw–claw and rotor core leakage paths, the field winding leakage inductance was calculated to be 45 mH. To compare with a measured value, the rotor was removed from the stator housing and the field winding inductance was measured to be 53 mH, which matched well with the calculated value.

V. Model Implementation

In many applications, the claw-pole alternator is connected to a 6-pulse rectifier as shown in Fig. 8. To validate the lumped-parameter model, a machine/rectifier simulation was implemented using the state-model-based simulation language ACSL [9]. The state model of the machine/rectifier was established using the Automated State Model Generation Algorithm (ASMG) derived in [10]. In the application of the ASMG, a system is described by pertinent branch parameters and circuit topology, similar to the syntax used in commercial circuit analysis programs, including Saber [11] and Spice [12]. The composite-system state equations are established algorithmically, and are solved using standard numerical integration algorithms.

In the initial study, the stator windings were connected in a delta-configuration and the rotor speed was held constant at 1800 rpm. A load resistance of 0.24 Ω was connected to the dc output terminals. The measured and simulated steady-state field current, phase current, and dc current are shown in Fig. 9. The measured and simulated electromagnetic torque is shown in Fig. 10. The measured torque was obtained using a two step procedure. In the first step, the rotor speed was held fixed with the

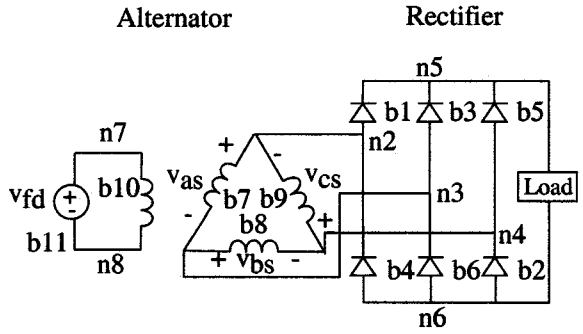

Fig. 8. Alternator/rectifier system.

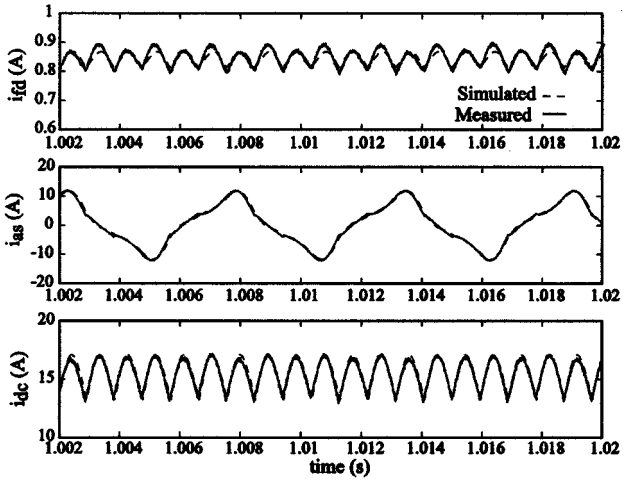

Fig. 9. Steady-state field current, phase current, and dc current.

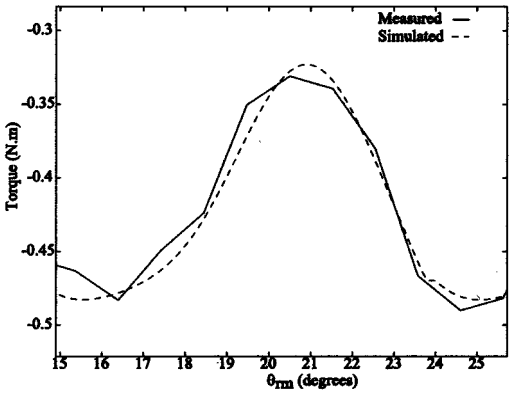

Fig. 10. Steady-state electromagnetic torque.

0.24 Ω load connected to the dc terminals. The stator and field currents were then measured with respect to rotor position. Once the measured values of current versus rotor position were obtained, the machine was stopped and the rectifier disconnected from the terminals. Individual power supplies were then placed across each of the stator windings and the field winding. The rotor was then locked at an arbitrary angle. Using the individual power supplies, the stator and field currents were adjusted to the values that were measured at the respective angle when the machine was running with the rectifier connected. The torque was

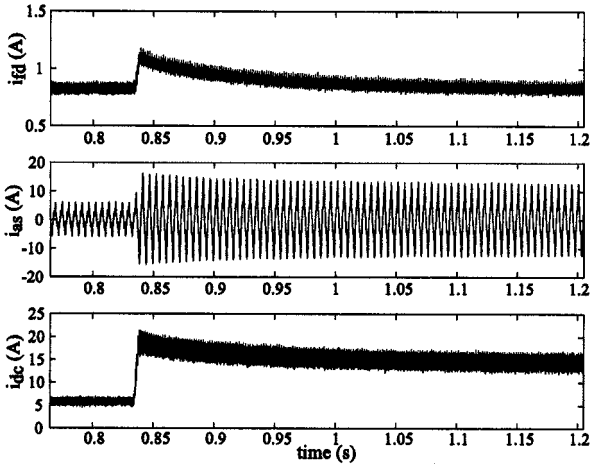

Fig. 11. Measured field, phase, and dc currents.

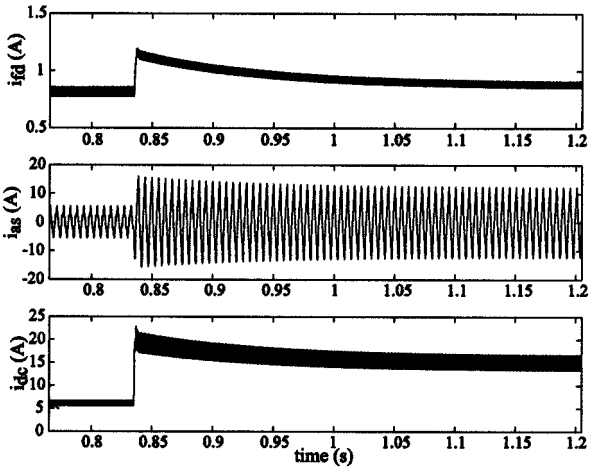

Fig. 12. Simulated field, phase, and dc currents.

then measured using an in-line torque transducer. The measurement was repeated at one degree (mechanical) increments. From Fig. 10 it can be seen that the torque is not constant in steady state. Rather, a torque ripple, resulting from harmonics introduced by rectification, current and back emf harmonics, as well as cogging torque is apparent. Nonetheless, comparing the measured and simulated responses it is seen that the torque ripple is well predicted.

In calculating the response, a fourth-order Runge–Kutta–Fehlberg algorithm was used with a maximum and minimum time step of 1×10^{-4} and 1×10^{-8}, respectively. The local truncation error, which is used to determine the actual time step, was set to 1×10^{-4} for all state variables. The simulation required approximately 1 s of CPU time to obtain 0.02 s of the dynamic response using a 450 MHz Pentium PC.

In the second study, it was assumed that the system was initially operating in the steady state with a base load resistance of 1 Ω connected to the dc output terminals. A second load resistance of 0.2 Ω was then connected in parallel with the original load. The measured response is shown in Fig. 11. The simulated response is depicted in Fig. 12. As shown, the measured and simulated transient responses are in very good agreement.

VI. Summary

A lumped-parameter coupled-circuit model of a claw-pole alternator is derived. The machine model is implemented in the simulation and analysis of an alternator/rectifier system using a state-model-based circuit analysis program. Comparisons with experimental results demonstrate the accuracy of the model in predicting the steady state and transient performance of the machine.

References

[1] I. Ramesohl, G. Henneberger, S. Kuppers, and W. Hadrys, "Three dimensional calculation of magnetic forces and displacements of a claw-pole generator," *IEEE Trans. Magn.*, vol. 32, pp. 1685–1688, May 1996.

[2] R. Wang and N. A. O. Demerdash, "Extra high speed modified lundell alternator parameters and open/short circuit characteristics from global 3D-FE magnetic field solutions," *IEEE Trans. Energy Conv.*, vol. 7, pp. 330–341, June 1992.

[3] B. H. Chen, J. D. Cote, and M. L. Hull, "Claw-pole generator simulation with Ansys/Saber for performance and noise improvement," presented at the Ansys Users Conference, 1997.

[4] S. Kuppers and G. Henneberger, "Numerical procedures for the calculation and design of automotive alternators," *IEEE Trans. Magn.*, vol. 33, pp. 2022–2025, Mar. 1997.

[5] H. Bai, "Alternator finite element simulation," Delphi Auto. Syst., Troy, MI, Tech. Presentation, 2000.

[6] V. Ostovic, J. M. Miller, V. Garg, R. D. Schultz, and S. Swales, "A magnetic equivalent circuit based performance computation of a Lundell alternator," *IEEE Trans. Ind. Applicat.*, vol. 35, pp. 825–830, July/Aug. 1999.

[7] M. Hecquet and P. Brochet, "Modeling of a claw-pole alternator using permeance network coupled with electric circuits," *IEEE Trans. Magn.*, vol. 31, pp. 2131–2134, May 1995.

[8] P. C. Krause, O. Wasynczuk, and S. D. Sudhoff, *Analysis of Electric Machinery*. Piscataway, NJ: IEEE Press, 1995.

[9] *Advanced Continuous Simulation Language Reference Manual*, Mitchell and Gauthier Associates, Concord, MA, 1993, pp. 1–3.

[10] O. Wasynczuk and S. D. Sudhoff, "Automated state model generation algorithm for power circuits and systems," *IEEE Trans. Power Syst.*, vol. 11, pp. 1951–1956, Nov. 1996.

[11] Analogy, Inc., "Introduction to the Saber Simulator," Analogy, Inc., Berkeley, CA, 1991.

[12] L. W. Nagel and D. O. Pederson, "Simulation program with integrated circuit emphasis," Univ. California Electron. Res. Lab., Memo. EAL-M382, 1973.

[13] R. L. Wiseman, "Graphical determination of magnetic fields with practical applications to salient-pole machine design," *Trans. AIEE*, pp. 430–437, May 1927.

[14] B. Heller and V. Hamata, *Harmonic Field Effects in Induction Machines*. New York: Elsevier, 1977.

Hua Bai (S'00) was born in Sa Mao, Yunnan, China, in 1972. He received the B.S. degree in electrical engineering from Tsinghua University, Beijing, China, and the M.S. degree in electrical engineering from the China Academy of Railway Sciences, Beijing, in 1995 and 1998, respectively. He is currently pursuing the Ph.D. degree in electrical engineering at the University of Missouri-Rolla. His interests are the analysis, simulation, and design of electric machines and drive systems.

Steven D. Pekarek (S'89–M'96) was born in Oak Park, IL, on December 22, 1968. He received the B.S.E.E., M.S.E.E., and Ph.D. degrees in electrical engineering from Purdue University, West Lafayette, IN, in 1991, 1993, and 1996, respectively.

Currently, he is an Assistant Professor of Electrical Engineering at the University of Missouri-Rolla. His interests include electric machines, numerical analysis, and automatic control.

Jerry Tichenor (S'96–M'96) received the B.S. degree (summa cum laude) and the M.S. degree in electrical engineering from the University of Missouri-Rolla, in 1994 and 1996, respectively.

Currently, he is a Research Engineer at the University of Missouri-Rolla. His research interests include power electronics and motor drives.

Walter Eversman received the B.S. degree from Purdue University, West Lafayette, IN and the Ph.D. degree from Stanford University, Stanford, CA, in 1959 and 1964, respectively.

He is Curators Professor of Mechanical and Aerospace Engineering at the University of Missouri-Rolla. His research interests include aeroacoustics and structural dynamics. He is a registered Professional Engineer in Missouri.

Duane J. Buening was born in Greensburg, IN, on January 26, 1964. He received the B.S. degree in mechanical engineering from Rose Hulman Institute of Technology, Terre Haute, IN, in 1986.

He is currently working in the Generator Design Analysis Group at Delphi Automotive Systems, Troy, MI. His focus is primarily on noise and vibration.

Gregory R. Holbrook was born in Hamilton, OH, on July 9, 1959. He received the B.S. degree in mechanical engineering from the University of Cincinnati, Cincinnati, OH, in 1982.

Currently, he is a Senior Project Engineer at Delphi Automotive Systems, Troy, MI. His interests include analytical structural analysis and experimental noise and vibration testing.

Michael L. Hull was born on November 29, 1951. He received the B.S. degree in mechanical engineering from Purdue University, West Lafayette, IN, and the M.S. degree in manufacturing management from Kettering University, Flint, MI, in 1974 and 1990, respectively.

Currently, he is a Supervisor in the Generator Design and Analysis Group, Delphi E & C Division, Delphi Automotive Systems, Troy, MI. This group's activities cover NVH and FEA analysis of generators.

Ronald J. Krefta was born in Buffalo, NY. He received the B.S. and M.S. degrees in electrical engineering from Purdue University, West Lafayette, IN, in 1984 and 1985, respectively.

Currently, he is working for Delphi Automotive Systems, Troy, MI, as a Design Engineer, concentrating on the design of electric machines for vehicle charging systems and hybrid vehicle applications.

Steven J. Shields was born in Xenia, OH, on July 11, 1956. He received the B.A. degree in biology from Anderson University, Anderson, IN, and the B.S. degree in mechanical engineering from Michigan State University, East Lansing, MI, in 1978 and 1986, respectively.

Currently, he is a Senior Project Engineer with the Generator Product Group, Delphi Energy & Chassis Division, Delphi Automotive Systems, Troy, MI.